JOURNAL OF THEORETICAL AND APPLIED MECHANICS
61, 2, pp. 343-354, Warsaw 2023
https://doi.org/10.15632/jtam-pl/162991

STUDY ON TENSILE FRACTURE FAILURE OF A STEEL PLATE WITH A SURFACE CRACK

Zhewen Chong, Jing Tao
School of Mechanical and Electrical Engineering, Hubei Polytechnic University, Huangshi, China
e-mail: 1340274972@qq.com; 605119917@qq.com
Yuehui Xie, Dongrong Wu
PipeChina Southwest Pipeline Co., Ltd, Jinniu District, Chengdu, China
e-mail: glitterx@163.com; 1743072567@qq.com
Tao Li
School of Mechanical and Electrical Engineering, Hubei Polytechnic University, Huangshi, China
e-mail: 30504935@qq.com

In order to study the effect of different surface crack parameters on the fracture failure of steel plate, the model was established by FEM. The results showed that the edge surface crack has the greatest influence on the fracture failure of the steel plate, and for non-edge surface cracks, the central surface crack has the greatest influence on the fracture failure of the steel plate. The larger the a/t and the smaller the a/c, the easier the steel plate fracture failure occurs. The a/c has a certain influence on the variation law of K and the position where K_{max} appears.

Keywords: steel plate, surface crack, stress intensity factor (SIF), fracture failure

1. Introduction

With the development of industrial production and large-scale steel structures, the market demand for steel plates is increasing day by day, and new requirements are also being put forward for the production quality of steel plates, not only to improve the yield of steel plates, but also to improve their quality. During the production and use of steel plates, surface cracks will inevitably occur due to material defects, rolling deformation and other factors (Yuan *et al.*, 2021). The surface cracks seriously affect the quality and yield of steel plates. The existence of cracks will accelerate the fracture failure, which may lead to major accidents (Wen, 2020). A steel plate with surface cracks as presented in Fig. 1. Hence, it is necessary to further study the fracture failure of steel plates containing crack defects.

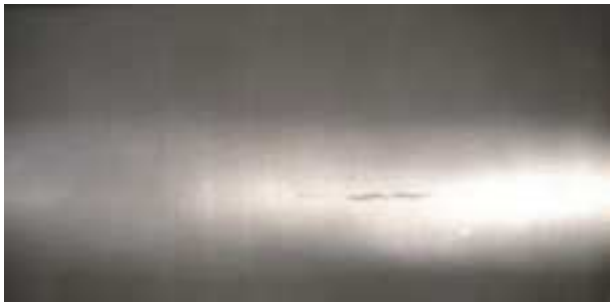

Fig. 1. The steel plate with a surface crack

In recent years, some scholars have done a lot of research on the fracture failure of steel plates and their repair, but there are relatively few studies on the fracture failure with surface crack defects. Dolbow *et al.* (2000) improved the extended finite element method (XFEM), then considered a discontinuous and a near tip strengthening function, applied it to the plate fracture problem, and verified the accuracy and practicability of the new formula. Lin and Smith (1999) analyzed a plate with a surface crack by using the finite element method. By estimating the stress intensity factor at the crack tip, the effects of the stress intensity factor on sensitivity of the crack shape, grid orthogonality and J-integral path independence were discussed. Saber *et al.* (2020) studied the influence of cutout size, position and geometry on the AISI1045 steel plate fatigue life and crack propagation path. The research showed that the cutout size and position were important parameters affecting crack propagation paths, and the increase or decrease in fatigue life could be predicted by cutout characteristics. Cheng *et al.* (2021) studied the fatigue crack propagation mechanism of carbon steel plate by using molecular dynamics (MD) and extended finite element methods (XFEM). Zhang *et al.* (2019) studied the effect of corrosion on fracture toughness of steel plates and found that the uniform and pitting corrosion damage would reduce the residual fracture toughness of corroded steel. Zhang *et al.* (2018) used Abaqus software to study deformation behavior of typical steel and analyzed the displacement change of the material during the shearing process. He *et al.* (2020) studied the causes of abnormal tensile fractures of steel plates through metallographic microscopes, scanning electron microscopes and energy dispersive spectrometers, and concluded that the main reason for abnormal tensile fractures were surface cracks. Zhang *et al.* (2021) used a fully coupled elastoplastic damage model with stress-state dependence to predict edge fracture during punching of high-strength steel plates. The results showed that the model prediction results were in good agreement with the experimental results. Chandra *et al.* (2020) used single edge notched tensile (SENT) specimens to evaluate the ductile tearing resistance of interstitial free steel plates and investigated the critical crack tip opening angle (CTOA) as well as the crack initiation parameters. Di Gioacchino *et al.* (2021) used a side-grooved Charpy test to evaluate the splitting and fracture properties of high-toughness steel plates. The research showed that the modified geometry could prevent the accumulation of plastic deformation under upper shelf energy temperature and improve the accuracy of impact performance measurement. Lee *et al.* (2022) used the finite element method and an experimental method to study the cause of random crack formation and propagation in high-alloy steels. The results showed that the alloy steel slabs were subjected to large thermal stresses during cooling. When chromium and boron were added, the possibility of a steel plate fracture increased. Omiya *et al.* (2022) studied the influence of material strength and notch shape on crack initiation and propagation characteristics of an AHSS sheet of a car body structure. The research showed that the crack generation and propagation behavior largely depended on the material strength and notch root radius. Li *et al.* (2020) studied the reinforcement effect of a fiber-reinforced polymer (FRP) on steel plates with surface cracks and proposed the optimal bond length and repair layer number. Liu *et al.* (2023) proposed an analytical model based on linear elastic fracture mechanics to evaluate fatigue performance of prestressed CFRP strip-reinforced steel plates. The research revealed that the proposed model coild better predict the stress state, stress intensity factor amplitude, fatigue crack growth life and the minimum pre-stress in the CFRP strip required for crack cessation under different strengthening conditions for various members.

However, those studies mainly focused on the fracture failure of steel plates and their repairs, while there are few studies on the fracture failure of steel plates with surface crack defects. The failure of steel plates with different crack positions, crack depth ratios and crack aspect ratios is not sufficiently analyzed. Hence, a steel plate with a surface crack is taken as the research object, and the influence of different crack positions, crack depth ratios and crack aspect ratios on the fracture failure is analyzed.

2. Theoretical method

2.1. *J*-integral and stress intensity factor

Rice (1968) proposed that the J-integral did not depend on the integral path around the crack. The J-integral is a fracture parameter to deal with nonlinear fracture problems. It does not need to calculate the elastic-plastic stress and strain fields near the crack tip, and it can be used for elastic and plastic evaluation. The J-integral can be expressed as

$$J = \int_{\Gamma} \left(w dy - T \frac{\partial u}{\partial x} ds \right) \tag{2.1}$$

where Γ is a curve surrounding the crack tip. The integral is calculated in a counter clockwise sense taking from the lower crack surface and continuing along the path Γ to the upper crack surface. w is strain energy density, u is the displacement vector, T depends on the outward normal n_j along Γ, $T = \sigma_{ij} n_j$, and ds is an arc length increment along Γ.

For cracks in linear elastic materials under mode I loading, the relationship between the J-integral and stress intensity factor K_I is as follows

$$K_I^2 = E' J \tag{2.2}$$

For the model subject to plane strain loading, E' can be expressed by equation $(2.3)_1$, and for the model subject to plane stress loading, E' can be expressed by equation $(2.3)_2$

$$E' = \frac{E}{1 - \nu^2} \qquad E' = E \tag{2.3}$$

where E is Young's modulus, ν is Poisson's ratio.

2.2. Crack propagation criterion

In the elastic-plastic state, the stress and strain near the crack tip can be uniquely determined by the J-integral. When the stress and strain field at the crack tip reaches the critical state of crack growth, the J-integral also reaches the critical value, and the crack will be unstable and start to grow. Therefore, the J-integral can be used as a fracture criterion for elastic-plastic cracked bodies. The J-integral fracture criterion can be expressed as

$$J \geqslant J_{IC} \tag{2.4}$$

where J_{IC} is the characteristic parameter of the material, also called the fracture toughness.

For the stress intensity factor, when it reaches the K_{IC} value, the crack will also appear unstable and then initiate crack propagation. The fracture criterion can be expressed as

$$K \geqslant K_{IC} \tag{2.5}$$

where K_{IC} is the characteristic parameter of the material, also called the fracture toughness.

3. Materials and methods

3.1. Steel plate geometric model and parameters

The finite element model of a steel plate is established with Q235. The main parameters of the steel plate are: length $L = 1000\,\text{mm}$, width $W = 500\,\text{mm}$, thickness $t = 12\,\text{mm}$, density $\rho = 7800\,\text{kg/m}^3$, Young's modulus $E = 210\,\text{GPa}$, Poisson's ratio $\mu = 0.3$, yield strength

$\sigma_s = 243\,\text{MPa}$, and tensile strength $\sigma_b = 465\,\text{MPa}$ (Zhang, 2020). Considering the tensile fracture failure of the steel plate with crack defects, the tensile load is set as $\sigma = 10\,\text{MPa}$. The tensile load is set at one end of the steel plate, and the other end is set with a fixed constraint. The steel plate model with a surface crack and a sectional view of the steel plate are presented in Fig. 2.

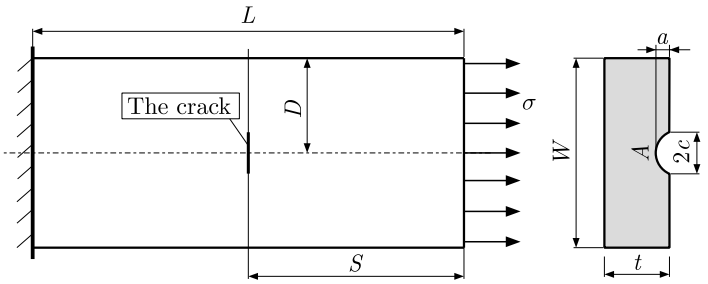

Fig. 2. Steel plate model with a surface crack and a sectional view of the steel plate

3.2. Finite element model

The steel plate with a surface crack has been implemented into the finite element software. In the process of crack propagation, any crack with an initial shape will gradually form a semi-elliptical crack (Shahani *et al.*, 2010; Anderson, 2017). Therefore, the semi-elliptical surface crack is used in the analysis. The actual field picture of the semi-elliptical crack is shown in Fig. 3a. The geometry of the semi-elliptical surface crack is shown in Fig. 3b. The dimension

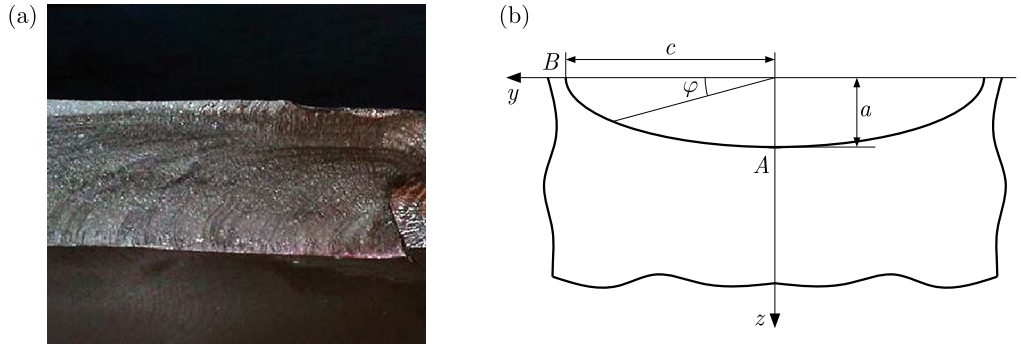

Fig. 3. The semi-elliptical crack: (a) actual photograph of a semi-elliptical crack and (b) semi-elliptical surface crack characterization

parameters φ, a and c are the crack angle, crack depth and a half of the crack length, respectively. For the surface crack, the surface point B is for the crack angle of 0°, and the deepest point A of the crack is for the crack angle of 90°. The crack depth ratio $a/t = 0.5$ and the crack aspect ratio $a/c = 0.5$ are defined for the initial crack located in the middle of the steel plate, as shown in Fig. 2. For the steel plate model with surface cracks, eight-node reduced-integration "brick" elements (C3D8R) have been adopted for the overall model. In order to eliminate singularity, the singular elements (Barsoum, 1975; Henshell and Shaw, 1975) were adopted for the crack front, and ten-node quadratic tetrahedron elements (C3D10) were used in the transition area between the crack front and the steel plate. The stress intensity factor (SIF) of the surface crack was calculated by using the contour integration method (Chong *et al.*, 2021). The finite element mesh of the steel plate is shown in Fig. 4.

In order to verify the effect of mesh number on the analysis results (Figiel and Kamiński, 2009), the mesh independence has been verified based on the initial cracking model of the steel plate. Three finite element models with different mesh numbers were established for analysis. The

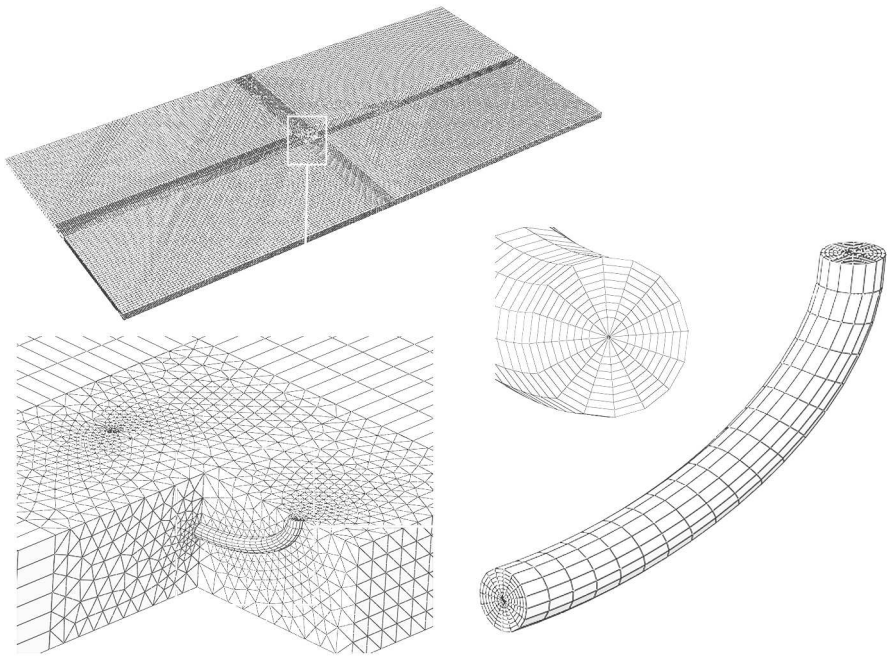

Fig. 4. Finite element mesh of the steel plate

mesh numbers in Mesh 1, Mesh 2 and Mesh 3 were 104188, 186451 and 399282, respectively. The SIF of the surface crack K with different mesh numbers is shown in Fig. 5. It can be clearly found that the crack SIFs of Mesh 1, Mesh 2, and Mesh 3 are almost the same, and the difference between them is very small. Therefore, increasing the number of meshes has little effect on the calculation results. The number of Mesh 2 meets the requirements of calculation accuracy. Considering the large number of meshes, the analysis time is long. Hence, Mesh 2 is a mesh generation standard to achieve accurate results.

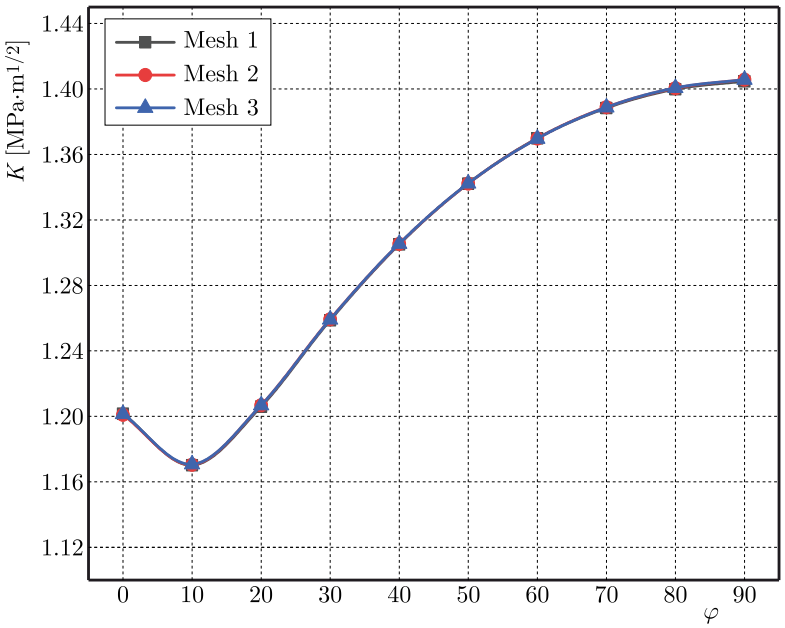

Fig. 5. The SIF of a crack for different meshes

3.3. Model validation

To verify the precision of the finite element calculation, we have calculated the SIF of the semi-elliptical surface crack with the initial crack depth ratio $a/t = 0.5$, crack aspect ratio $a/c = 0.5$. The crack is located in the middle of the steel plate, that is, $S/L = 0.5$, $D/W = 0.5$.

For an infinite center cracked plate subjected to uniform tensile stress at infinity, the stress intensity factor can be expressed as

$$K = \sigma\sqrt{\pi a} \tag{3.1}$$

where σ is the stress, a is the crack length.

For finite-sized components in the project, the stress intensity factor needs to be modified based on the above formula, so it can be expressed as

$$K = \sigma\sqrt{\pi a} f(a, W, \ldots) \tag{3.2}$$

where $f(a, W, \ldots)$ is a geometric correction coefficient.

Due to complexity of the problem, the analytical solution is still difficult to obtain for three--dimensional surface cracks. However, in order to meet the needs of solving practical engineering problems, Newman and Raju (1984) used the finite element method and numerical fitting to give an empirical formula for calculating the surface crack stress intensity factor. The theoretical calculation formula for the SIF K of a plate with semi-elliptical surface cracks can be expressed as (Newman and Raju, 1984)

$$K = \frac{\sigma\sqrt{\pi a}}{E(k)} F_s\Big(\frac{a}{c}, \frac{a}{t}, \frac{c}{w}, \varphi\Big) \tag{3.3}$$

where

$$E(k) = \sqrt{1 + 1.464\Big(\frac{a}{c}\Big)^{1.65}} \qquad F_s = \Big[M_1 + M_2\Big(\frac{a}{t}\Big)^2 + M_3\Big(\frac{a}{t}\Big)^4\Big] g f_\varphi f_w$$

$$M_1 = 1.13 - 0.09\frac{a}{c} \qquad M_2 = -0.54 + \frac{0.89}{0.2 + \frac{a}{c}}$$

$$M_3 = 0.5 - \frac{1}{0.65 + \frac{a}{c}} + 14\Big(1 - \frac{a}{c}\Big)^{24} \qquad g = 1 + \Big[0.1 + 0.35\Big(\frac{a}{t}\Big)^2\Big](1 - \sin\varphi)^2$$

$$f_\varphi = \sqrt[4]{\Big(\frac{a}{c}\Big)^2 \cos^2\varphi + \sin^2\varphi} \qquad f_w = \sqrt{\sec\Big(\frac{\pi c}{2W}\sqrt{\frac{a}{t}}\Big)}$$

Compared with the calculation results from equation (3.3), the finite element model results are very close, and the errors for different crack angles φ are less than 5%. The errors between simulation results and calculation formula are shown in Fig. 6.

4. Results and discussion

4.1. Effects of crack position on the SIF of a surface crack

The initial crack depth ratio is $a/t = 0.5$, and initial crack aspect ratio $a/c = 0.5$. Considering the influence of crack position on the SIF, D/W and S/L are defined to represent the crack position, and D/W and S/L represent the width and length ratios of the position in the steel plate where the crack is located, respectively. The length ratio $S/L = 0.5$ is taken to analyze the changes in the SIF of the crack K at different crack angles φ when the width ratio is $D/W = 0$, 0.1, 0.2, 0.3, 0.4 and 0.5.

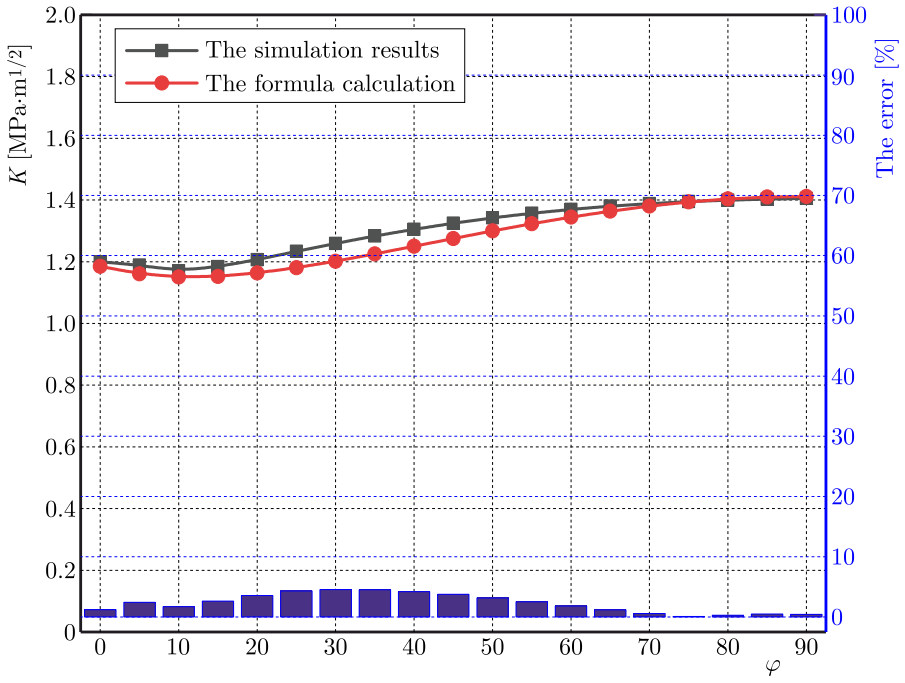

Fig. 6. The error value between simulation results and calculation formula

The variation of the crack SIF for different width ratios is shown in Fig. 7a. Firstly, K decreases and then increases gradually with an increase of φ. K gradually decreases within the crack angle range $\varphi = 0°$-$10°$, and then gradually increases within the range of $10°$-$80°$, and finally stabilizes after $80°$ when $D/W = 0$. K gradually increases within the crack angle range of $10°$-$90°$, and the increasing trend gradually stabilizes when $D/W = 0.1$-0.5. The maximum value of the SIF K_{max} for different width ratios appears at the deepest point of the crack $\varphi = 90°$. In order to further study the influence of width ratios D/W on K, K at the deepest point of the crack has been extracted for study. The variation of K at the deepest point of the crack is shown in Fig. 7b. K decreases first as the width ratio D/W increases, and then gradually increases. K gradually decreases in the range of width ratio $D/W = 0$-0.1, and gradually increases in the range of width ratio $D/W = 0.1$-0.5. K is the largest when $D/W = 0$, and the crack is an edge surface crack.

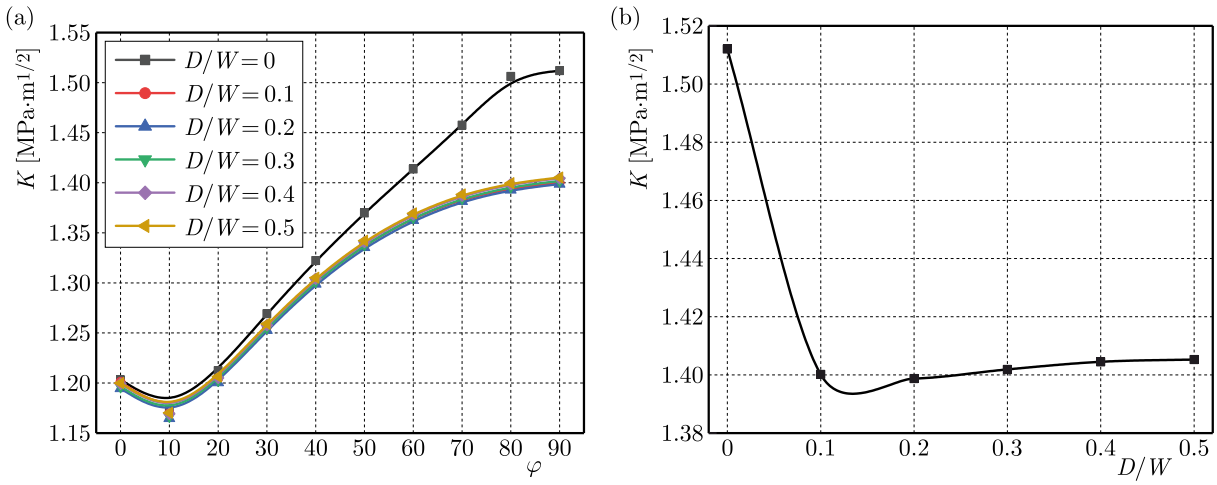

Fig. 7. The SIF of a crack for different width ratios: (a) variation of the crack SIF, (b) variation of SIF at the deepest point of the crack

As shown in Figs. 7a and 7b, the variation rule of K when the width ratio $D/W = 0$ is obviously different from that for $D/W = 0.1$, 0.2, 0.3, 0.4 and 0.5. K at the deepest point when $D/W = 0$ is much larger than that at the deepest point when $D/W = 0.1$, 0.2, 0.3, 0.4 and 0.5, indicating that the edge surface crack has the greatest influence on the fracture failure of the steel plate. K of a non-edge surface crack increases with an increase of D/W, and the maximum value of K appears at $D/W = 0.5$, that is, the central surface crack, which indicates that for a non-edge surface crack, the central surface crack has the greatest influence on the fracture failure of the steel plate.

Considering that the edge surface crack has the greatest influence on the fracture failure of the steel plate, the edge surface crack is selected to analyze the influence of different length ratios on the crack SIF, that is, the width ratio $D/W = 0$ and length ratios $S/L = 0.1$, 0.3, 0.5, 0.7 and 0.9 are taken to analyze the variation of K at different crack angles φ.

The variation of the crack SIF for different length ratios is shown in Fig. 8a. K firstly decreases and then increases gradually with an increase of φ. K gradually decreases within the crack angle range $\varphi = 0°$-$10°$, and K gradually increases within the range of $10°$-$80°$, then in tends to be stable above $80°$. The maximum value of the SIF K_{max} appears at the deepest point of the crack $\varphi = 90°$. In order to further study the influence of length ratios S/L on K, K at the deepest point of the crack is extracted for study. The variation of K at the deepest point of the crack is shown in Fig. 8b. K firstly slowly decreases as the length ratio S/L increases, then gradually decreases, and the decreasing trend becomes larger. K decreases slowly in the range of length ratios $S/L = 0.1$-0.5, and the change of K value is small. K gradually decreases in the range of length ratios $S/L = 0.5$-0.9, and the decreasing trend is larger than that in the range of $S/L = 0.1$-0.5. K is the largest when $S/L = 0.1$, indicating that the closer is to the stress end, the larger K is.

As shown in Figs. 8a and 8b, the decreasing trend of K in the range of length ratios $S/L = 0.1$-0.5 is obviously different from that in the range of $S/L = 0.5$-0.9. The trend changes at $S/L = 0.5$ indicate that this is the inflection point of the trend change. When the length ratios are $S/L = 0.1$, 0.3 and 0.5, the variation rule of K is the same, and the variation of K is small. The maximum variation difference of K is $0.01\,\mathrm{MPa{\cdot}m^{1/2}}$, indicating that the edge surface cracks when $S/L \leqslant 0.5$, which has the greatest influence on the fracture failure of the steel plate.

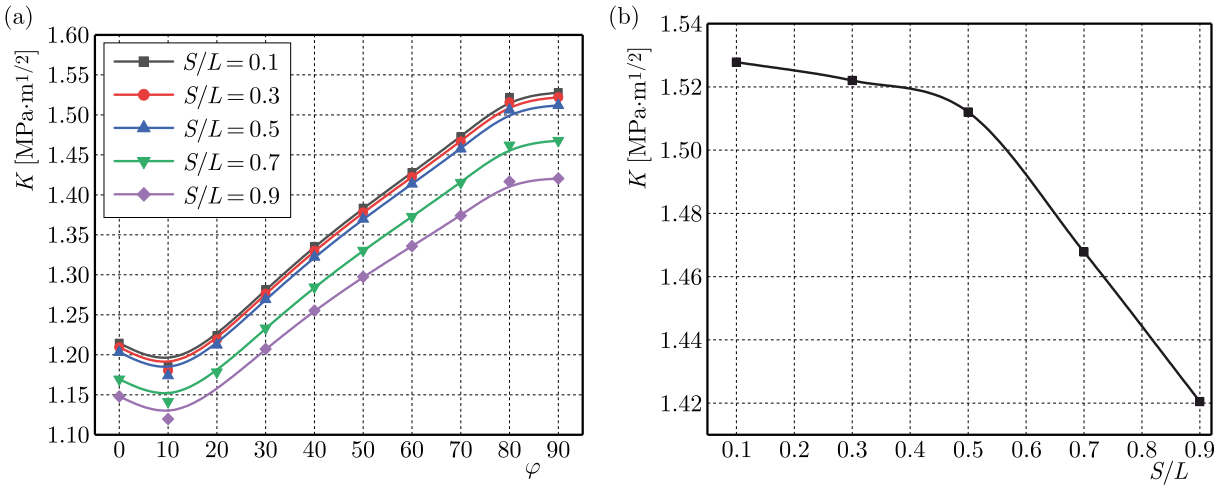

Fig. 8. The SIF of a crack for different length ratios: (a) variation of the crack SIF, (b) variation of SIF at the deepest point of the crack

Considering that the crack position has the greatest influence on the fracture failure of the steel plate when the width ratio $D/W = 0$ and the length ratio $S/L \leqslant 0.5$, the crack position

is selected in this paper when the width ratio $D/W = 0$ and the length ratio $S/L = 0.5$. The influence of different crack depth ratios and crack aspect ratios on the crack SIF is analyzed.

4.2. Effects of crack depth ratio on the SIF of a surface crack

To study the influence of crack depth ratio on the SIF of a surface crack, different depth ratios $a/t = 0.2$, 0.3, 0.4, 0.5 and 0.6 have been considered. Meanwhile, the crack aspect ratio $a/c = 0.5$ has been taken to analyze the variation of K at different crack angles φ.

The variation of the crack SIF for different crack depth ratios is shown in Fig. 9a. K firstly decreases and then gradually increases with an increase of φ. K gradually decreases within the crack angle range $\varphi = 0°$-$10°$, and gradually increases within the range of $10°$-$80°$, then it tends to be stable above $80°$. The maximum value of the SIF K_{max} appears at the deepest point of the crack $\varphi = 90°$.

In order to further study the influence of crack depth ratios a/t on K, K at the deepest point of the crack has been extracted for study. The variation of K at the deepest point of the crack is shown in Fig. 9b. K gradually increases as the crack depth ratio a/t increases, and the increasing trend of K becomes linear, indicating that the larger the crack depth ratio a/t, the more prone the steel plate is to fracture failure.

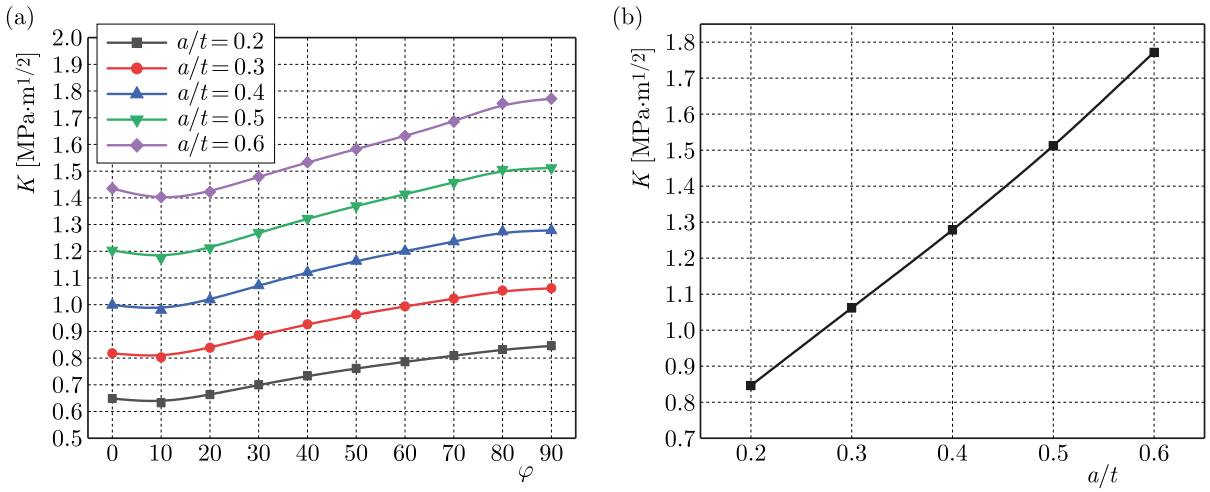

Fig. 9. SIF of a crack for different crack depth ratios: (a) variation of the crack SIF, (b) variation of SIF at the deepest point of the crack

4.3. Effects of the crack aspect ratio on the SIF of a surface crack

To study the influence of crack aspect ratio on the SIF of a surface crack, different aspect ratios $a/c = 0.3$, 0.4, 0.5, 0.6 and 0.7 have been considered. Meanwhile, the crack depth ratio $a/t = 0.5$ has been taken to analyze the variation of K at different crack angles φ.

The variation of the crack SIF for different crack aspect ratios is shown in Fig. 10a. When the crack aspect ratio is $a/c = 0.3$, K firstly rapidly increases and then decreases gradually with an increase of φ. K gradually increases within the crack angle range $\varphi = 0°$-$80°$, and then decreases gradually above $80°$. When the crack aspect ratio is $a/c = 0.4$, K first slowly increases with φ, then gradually increases, and finally gradually decreases. K increases slowly within the crack angle range $\varphi = 0°$-$10°$, and gradually increases within the range $\varphi = 10°$-$80°$, and then gradually decreases above $80°$. When the crack aspect ratio is $a/c = 0.5$, K slowly decreases with an increase of φ first, then gradually increases and tends to be stable. K decreases slowly within the range $\varphi = 0°$-$10°$, and gradually increases within $\varphi = 10°$-$80°$, then tends to be stable above $80°$. When the crack aspect ratio is $a/c = 0.6$, K firstly slowly decreases, and then

it increases gradually with an increase of φ. K decreases slowly within the range $\varphi = 0°$-$20°$, and gradually increases within $\varphi = 20°$-$90°$. When the crack aspect ratio is $a/c = 0.7$, K firstly decreases, and then increases gradually with an increase of φ. K gradually decreases within $\varphi = 0°$-$20°$, and gradually increases within the angles $\varphi = 20°$-$90°$. In order to further study the influence of crack aspect ratios a/c on K, K at the deepest point of the crack has been extracted for study. The variation of K at the deepest point of the crack is shown in Fig. 10b. K gradually decreases with an increase of the aspect ratio a/c, indicating that the smaller the crack aspect ratio is a/c, the steel plate is more prone to fracture failure.

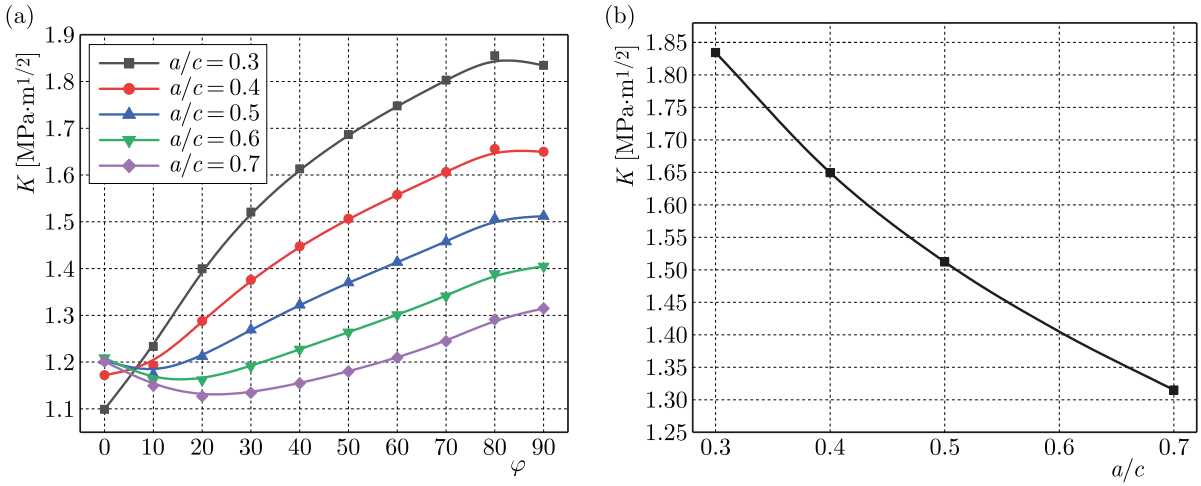

Fig. 10. SIF of a crack for different crack aspect ratios: (a) variation of the crack SIF, (b) variation of SIF at the deepest point of the crack

As shown in Figs. 10a and 10b, the variation rule of K when the crack aspect ratio is $a/c < 0.5$ is obviously different from that when $a/c \geqslant 0.5$, indicating that the crack aspect ratio has a certain influence on the variation of K at different crack angles φ. The maximum value of the SIF K_{max} appears at $\varphi = 80°$ when the crack aspect ratio is $a/c < 0.5$, and the maximum value of the SIF K_{max} appears at the deepest point of the crack $\varphi = 90°$ when the crack aspect ratio is $a/c \geqslant 0.5$, indicating that the crack aspect ratio has a certain influence on the position of the maximum value of the SIF K_{max}.

5. Conclusions

By analyzing the stress intensity factor of a steel plate with surface crack defects, the influence of different crack positions, crack depth ratios and crack aspect ratios on the stress intensity factor has been found. To a certain extent, the conclusions obtained in this paper can provide a theoretical reference for the fracture failure analysis of steel plates.

- The SIF K firstly decreases and then gradually increases with an increase of the width ratio D/W. The SIF K is the largest when $D/W = 0$, and the crack is an edge surface crack, indicating that the edge surface crack has the greatest influence on the fracture failure of steel plates. For a non-edge surface crack, K increases with an increase of the width ratio D/W, and the maximum value of K appears at $D/W = 0.5$, that is, the central surface cracks, indicating that for the non-edge surface crack, the central surface crack has the greatest influence on the fracture failure of the steel plate.
- The SIF K firstly slowly decreases as the length ratio S/L increases, then gradually decreases, and the decreasing trend becomes larger. The maximum value of K appears at $S/L = 0.1$, indicating that the closer is to the stress end, the larger K becomes. When

$S/L \leqslant 0.5$, the variation of K value is small, and the maximum variation difference of K value is 0.01 MPa·m$^{1/2}$. The change of K is large when $S/L \geqslant 0.5$, indicating that the edge surface cracks when $S/L \leqslant 0.5$, which has the greatest influence on the fracture failure of the steel plate.

- The SIF K gradually increases as the crack depth ratio a/t increases, and the increasing trend of K tends to be linear, indicating that the larger is the crack depth ratio a/t, the more prone the steel plate is to fracture failure.
- The variation rule of K when the crack aspect ratio is $a/c < 0.5$ is obviously different from that when $a/c \geqslant 0.5$, indicating that the crack aspect ratio has a certain influence on the variation rule of K at different crack angles φ. The position of the SIF K_{max} when the crack aspect ratio is $a/c < 0.5$ is different from that when $a/c \geqslant 0.5$, indicating that the crack aspect ratio has a certain influence on the position of the maximum value of the SIF K_{max}. K gradually decreases with an increase of the aspect ratio a/c, indicating that the smaller is the crack aspect ratio a/c, the more prone to fracture failure is the steel plate.

Acknowledgments

The authors are grateful for the support from the Youth Funding Project of Hubei Polytechnic University (No. 21xjz03Q) and the open project of Intelligent Transportation Technology and Equipment of Hubei Provincial Key Laboratory (No. 2020XZ109).

References

1. Anderson T.L., 2017, *Fracture Mechanics: Fundamentals and Applications*, CRC Press
2. Barsoum R.S., 1975, Further application of quadratic isoparametric finite elements to linear fracture mechanics of plate bending and general shells, *International Journal of Fracture*, **11**, 1, 167-169
3. Chandra S.K., Sarkar R., Bhowmick A.D., De P.S., Chakraborti P.C., Ray S.K., 2020, Evaluation of ductile tearing resistance of an interstitial free steel sheet using SENT specimens, *Engineering Fracture Mechanics*, **238**, 107257
4. Cheng Z., Wang H., Liu G.-R., 2021, Fatigue crack propagation in carbon steel using RVE based model, *Engineering Fracture Mechanics*, **258**
5. Chong Z., Ma T., Yu D., Wu D., Tao J., Lv H., 2021, Stress intensity factor of double cracks on seabed-spanning pipeline surface under the spring boundary, *Journal of Pipeline Systems Engineering and Practice*, **12**, 4
6. Di Gioacchino F., Lucon E., Mitchell E.B., Clarke K.D., Matlock D.K., 2021, Side-grooved Charpy impact testing: Assessment of splitting and fracture properties of high-toughness plate steels, *Engineering Fracture Mechanics*, **252**, 107842
7. Dolbow J., Moës N., Belytschko T., 2000, Modeling fracture in Mindlin-Reissner plates with the extended finite element method, *International Journal of Solids and Structures*, **37**, 48-50, 7161-7183
8. Figiel Ł., Kamiński M., 2009, Numerical probabilistic approach to sensitivity analysis in a fatigue delamination problem of a two-layer composite, *Applied Mathematics and Computation*, **209**, 1, 75-90
9. He Y., Li L., Lu Z., *et al.*, 2020, Analysis on abnormal tensile fracture of a certain high strength steel (in Chinese), *Materials Protection*, **53**, 2, 157-161
10. Henshell R.D., Shaw K.G., 1975, Crack tip finite elements are unnecessary, *International Journal for Numerical Methods in Engineering*, **9**, 3, 495-507

11. Lee Y.-S., Kim S., Jang D.-W., Lee S.-B., 2022, Mechanism of crack initiation and propagation in high-alloy steel slabs during the cooling and scarfing processes after the continuous casting process, *Mechanics of Materials*, **166**, 104240

12. Li Z., Jiang X., Hopman H., Zhu L., Liu Z., 2020, Numerical investigation on the surface crack growth in FRP-reinforced steel plates subjected to tension, *Theoretical and Applied Fracture Mechanics*, **108**

13. Lin X.B, Smith R.A., 1999, Finite element modelling of fatigue crack growth of surface cracked plates. Part I: The numerical technique, *Engineering Fracture Mechanics*, **63**, 503-522

14. Liu J., Xin H., Zhao X.-L., 2023, Prediction of fatigue crack propagation in center cracked steel plate strengthened with prestressed CFRP strip, *Thin-Walled Structures*, **183**, 110416

15. Newman Jr. J.C., Raju I.S., 1984, *Stress-Intensity Factor Equations for Cracks in Three--Dimensional Finite Bodies Subjected to Tension and Bending Loads*, National Aeronautics and Space Administration (NASA), Langley Research Center, Hampton, VA

16. Omiya M., Arakawa S., Yao Z., Muramatsu M., Nishi S., Takada K., Murata M., Okato K., Ogawa K., Oide K., Kobayashi T., Han J., Terada K., 2022, Influence of strength and notch shape on crack initiation and propagation behavior of advanced high strength steel sheets, *Engineering Fracture Mechanics*, **271**, 108573

17. Rice J.R., 1968, A path independent integral and the approximate analysis of strain concentration by notches and cracks, *Journal of Applied Mechanics*, **35**, 2, 379-386

18. Saber A., Shariati M.R., Nejad M., 2020, Experimental and numerical investigation of effect of size, position and geometry of some cutouts on fatigue life and crack growth path on AISI1045 steel plate, *Theoretical and Applied Fracture Mechanics*, **107**, 102506

19. Shahani A.R., Shodja M.M., Shahhosseini A., 2010, Experimental investigation and finite element analysis of fatigue crack growth in pipes containing a circumferential semi-elliptical crack subjected to bending, *Experimental Mechanics*, **50**, 5, 563-573

20. Wen Y., 2020, *Research on Fracture Performance of Corroded Steel Plate with Central Crack*, Xi'an: Xi'an University of Architecture and Technology

21. Yuan P., Fu D., Gao Y., *et al.*, 2021, Causes analysis and improvement measures for surface cracks of Q235B steel plate (in Chinese), *Wide ang Heavy Plate*, **27**, 6, 34-36

22. Zhang H., Xu S., Nie B., Wen Y., 2019, Effect of corrosion on the fracture properties of steel plates, *Construction and Building Materials*, **225**, 20, 1202-1213

23. Zhang K., Wang M., Liu W., Liu J., 2021, Fracture prediction for an advanced high-strength steel sheet using the fully coupled elastoplastic damage model with stress-state dependence, *Acta Mechanica Solida Sinica*, **34**, 263-273

24. Zhang Q., 2020, *Study on Mechanical Response of Q235 Steel and Constitutive Model under Cyclic Loading*, Hebei: Yanshan University

25. Zhang S.Q., Jiao S.H., Ding J.H., Zhang Q.F., Jiang H.S., 2018, Simulation study on shear crack of steel plate, *Materials Science Forum*, **941**, 480-485

Manuscript received May 1, 2022; accepted for print April 3, 2023